Actinide production from the interactions of ^{40}Ca and ^{44}Ca with ^{248}Cm and a comparison with the ^{48}Ca+^{248}Cm system

A. Türler* and H. R. von Gunten
Laboratorium für Radiochemie, Universität Bern, 3000 Bern 9, Switzerland

J. D. Leyba,† D. C. Hoffman, D. M. Lee, K. E. Gregorich, D. A. Bennett,‡ R. M. Chasteler,§ C. M. Gannett,** H. L. Hall,†† R. A. Henderson,‡‡ and M. J. Nurmia
Nuclear Science Division, Lawrence Berkeley Laboratory, Berkeley, California 94720
(Received 29 June 1992)

Excitation functions have been measured for production of isotopes of Th through Fm in bombardments of ^{248}Cm with 231- to 323-MeV ^{44}Ca ions and for the production of isotopes of Th through Cm in bombardments of ^{248}Cm with 230- to 291-MeV ^{40}Ca ions, respectively, using radiochemical methods. Upper production cross section limits were established for nuclides that were not positively detected. The experimental data were compared with the results of previous reaction studies in the systems ^{40}Ca+^{248}Cm and ^{48}Ca+^{248}Cm. The half-widths of the Gaussian isotopic distributions were about 2.5 mass numbers for above-target elements and 5 to 5.5 mass numbers for below-target elements in all three systems. The majority of the cross section for the production of above-target nuclides was assigned to predominantly quasielastic reactions, whereas below-target nuclides were formed in deeply inelastic and asymmetric quasifission reactions. The maxima of the isotopic distributions were shown by others to closely follow the minimum of the potential energy surface in experiments with ^{48}Ca, whereas in reactions with ^{40}Ca and ^{44}Ca we found that a transfer of 4 to 5 protons in either direction was required to reach the minimum in potential energy. The different neutron numbers of ^{40}Ca, ^{44}Ca, and ^{48}Ca are only partly reflected in the target-like reaction products. Based on a simple model, excitation energies and the maxima of the excitation functions were calculated and compared with the actual data. The yields for production of the below-target elements Th, U, and Pu were found to be two orders of magnitude smaller in the reaction of ^{40}Ca with ^{248}Cm than with ^{48}Ca. The differences for production of above-target elements were largest between the reactions of ^{44}Ca and ^{48}Ca ions with ^{248}Cm. Differences in below-target yields have been attributed either to losses of reaction products due to prompt fission, and/or to dynamic effects due to fusion hindrance. The data for above-target elements seem to confirm the presence of a strong isospin driving force, which in combination with favorable reaction energies results in surprisingly high yields in reactions with ^{44}Ca projectiles.

PACS number(s): 25.70.Hi, 25.70.Jj, 27.90.+b

I. INTRODUCTION

In recent years much interest has been focused on heavy-ion-induced transfer and fusion reactions. Heavy-ion reactions of actinide targets ranging from ^{238}U to ^{254}Es with a variety of projectiles ranging from ^{16}O to ^{238}U have been studied [1–17]. The fact that ^{248}Cm is the heaviest long-lived and neutron-rich nuclide available in multimilligram quantities has rendered it a very popular target material [3–7,9,10,15–17]. One reason for these studies is the possibility of transferring large numbers of nucleons between the projectile and the target nucleus or even fusing the target and projectile. As a result, neutron-rich and neutron-deficient actinide and transactinide nuclides may be produced for study of their decay properties as well as their chemical behavior. These nuclides are inaccessible with other types of reactions, such as neutron-capture or light-ion stripping reactions. However, the production of these exotic nuclides by means of transfer reactions is rather unspecific. Usually extensive radiochemical separations must be applied to isolate them. The present study is part of a continuing effort to systematically investigate various projectile-target combinations, and to broaden the present understanding of transfer reactions. As yet, the quantitative description of the evolution of a heavy-ion reaction is beyond the reach of present transport theories [18–21].

Another reason for these studies is the hope of using heavy-ion transfer or fusion reactions to produce new, very heavy or even superheavy elements in the vicinity of

*Present address: Chemistry Division, Paul Scherrer Institute, CH-5232 Villigen, Switzerland.
†Present address: Westinghouse Savannah River Co., Savannah River Laboratory, Bldg. 773 A, Aiken, SC 29808.
‡Present address: Division of New Technology, Materials & Research, Office of Environmental & Engr., Chemistry Branch, Sacaramento, CA 95819.
§Present address: Department of Physics, Duke University, Durham, NC 27706.
**Present address: Orange County Sheriffs Dept., Santa Ana, CA 92701.
‡Present address: Nuclear Chemistry Division, Lawrence Livermore National Laboratory, Livermore, CA 94550.
‡‡Present address: EG&G Rocky Flats, Inc., Rocky Flats Plant, Golden, CO 80402.

the predicted island of stability at $Z=114$ and $N=184$. So far the most promising attempt to fuse the doubly magic projectile ^{48}Ca with the magic heavy neutron-rich ^{248}Cm failed to yield evidence for fusion evaporation residues. Cross section limits for these reactions of 10^{-34}–10^{-35} cm^2 were found, within a half-life window between microseconds and years [22]. This result allows a number of interpretations. It may be that the resulting compound nucleus is entirely lost by prompt fission, or, that the fusion of this system is dynamically hindered at energies near the Coulomb barrier. The fusion probability of this system at the Bass model fusion barrier may be calculated to be on the order of 3×10^{-4} (Ref. [23]), which corresponds to a considerable fusion hindrance. Many authors have shown that with increasing hindrance of fusion a new reaction channel opens, the so-called "quasifission" or "fast-fission" channel. Then, at energies near the barrier, a strong transfer of mass from the projectile to the target nucleus occurs, resulting in nearly equal mass products [24–29]. A radiochemical study of target-like products in reactions of ^{48}Ca ions with ^{248}Cm showed a strong tendency for massive transfers of nucleons from target to projectile [9]. Evidence was put forward that in asymmetric quasifission reactions these below-target nuclides are produced with very little excitation energy, whereas the complementary light fragments seem to be highly excited [28]. The production cross sections for above-target nuclides were highest for transfers of a few nucleons and decreased rapidly with an increase in the number of nucleons transferred. These results were compared with a study [6] of the reactions of the neutron-deficient, but also doubly magic projectile, ^{40}Ca, with ^{248}Cm. Similar maximum production cross sections resulted for the above-target elements. The eight fewer neutrons in the ^{40}Ca projectile were only partially reflected in the mass distributions for a given Z. In contrast, so far unpublished results for below-target elements obtained by Lerch [30] indicate that the production cross sections rapidly drop off to a level about 100 times lower than the yields observed with ^{48}Ca projectiles. This unexpected behavior seems to indicate a pronounced one-directional transfer of protons from the neutron-deficient projectile to the target nucleus in the early stages of the interaction. A similar result has been observed by de Souza *et al.* [18] in the reactions of ^{40}Ca with ^{238}U.

The primary product mass and charge distributions are thought to be strongly influenced by the underlying potential energy surface (PES) [18–20]. The PES reflects the potential energy between the initial target-projectile combination (the injection point in the PES) and a vast number of possible transfer reaction products. The most probable product mass arrangement should occur when the density of states in the dinuclear complex is largest, which corresponds to a minimum of the potential energy in the system [31]. Thus, the strongest driving force for nucleon transfer should point from the injection point in the PES in the direction that minimizes the potential energy of the system. The use of ^{40}Ca projectiles introduces a steep gradient in the charge and mass degree of freedom in the vicinity of the injection point [18], whereas the PES with ^{48}Ca projectiles exhibits a rather small local gradient [9,20]. In fact, the injection point coincides with a local minimum in the PES. Nucleon transport theories fail to predict quantitatively the evolution of the mass and charge distributions when steep gradients in the potential energy surface are involved [18,21].

The aim of the present research was to complete the unpublished results of Lerch [30] for below-target yields in the reactions of ^{40}Ca+^{248}Cm and to investigate the new reaction system ^{44}Ca+^{248}Cm, which exhibits only a moderate local gradient in the charge and mass degree of freedom of the PES at the injection point and, therefore, can be regarded as a transition system between the two extremes. In addition, ^{44}Ca has a neutron number of 24, which is half way between the magic neutron numbers 20 and 28, of the doubly magic nuclei ^{40}Ca and ^{48}Ca, respectively. Therefore, ^{44}Ca can be used to study the influence of neutron shell effects on the final isotopic distributions of the actinide products. Using radiochemical separation techniques, excitation functions have been determined for isotopes of Am in the reactions of ^{40}Ca+^{248}Cm at energies between 0.98 and 1.24 times the nominal Coulomb barrier (E_{Coul}). Upper limits on the production cross sections have been established for nuclides that have not positively been detected. In the system ^{44}Ca+^{248}Cm excitation functions for isotopes of Th through Fm have been measured at energies between $0.98E_{\mathrm{Coul}}$ and $1.37E_{\mathrm{Coul}}$.

II. EXPERIMENTAL

A. Target arrangement

Irradiations of ^{248}Cm with ^{40}Ca and ^{44}Ca ions were performed at the Lawrence Berkeley Laboratory 88-Inch Cyclotron, which is specially equipped to safely irradiate highly radioactive target materials. The isotope ^{44}Ca has a natural abundance [32] of 2.09 atom % and 600 mg were obtained from Oak Ridge National Laboratory as separated ^{44}Ca (98.6 atom %) in the metallic form. Typical beam intensities were >100 particle nA. The target arrangement used for the irradiations has been described previously [15]. The beam, after being collimated by a water-cooled graphite ring, passed through a 1.8-mg/cm^2 Havar foil (composition Co 42.5%, Cr 20.0%, Fe 17.9%, Ni 13.0%, W 2.8%, Mo 2.0%, Mn 1.6%, C 0.2%, Be 0.04%), which isolates the target chamber from the vacuum of the beam line. The beam then passes through a volume of 0.2-mg/cm^2 nitrogen cooling gas and the 2.75-mg/cm^2 Be target backing before interacting with the Cm target. The target contained 644 μg/cm^2 of ^{248}Cm in the form of Cm_2O_3 (97.44% ^{248}Cm, 0.010% ^{247}Cm, 2.53% ^{246}Cm, 0.025% ^{245}Cm, and 10^{-4}% ^{244}Cm) and was prepared as a 7-mm-diameter circle by stepwise electrodeposition of $Cm(NO_3)_3$ from an isopropanol solution on the Be foil. Each deposited layer was converted to the oxide by heating to 300 °C. The thickness of the Cm target was monitored by alpha spectroscopy.

Reaction products recoiling from the target were stopped in 5.7–7 mg/cm^2 Cu catcher foils that were processed immediately after the irradiations. The catcher foils subtended laboratory angles between 0° and 60° to

the beam axes [0° to 130° in the center of mass (c.m.) system]. The thickness of the catcher foils was calculated to be sufficient to stop all reaction products with full forward momentum transfer. Unreacted beam ions passed through the catcher foil and were stopped in a water-cooled beam stop. The sum of the electrical current deposited in the Havar isolation foil, the target, the recoil catcher foil, and the beam stop was measured with an integrating electrometer and recorded periodically in order to reconstruct the irradiation history. Typical irradiation times were from 6 to 8 h.

The energy lost by the projectiles while passing through the Havar isolation foil, the nitrogen cooling gas, the Be target backing, and the target material was calculated using the range and stopping power tables of Hubert *et al.* [33]. Since only values for pure elements are tabulated the stopping power of Havar and Cm_2O_3 have to be approximated. The stopping power of Havar was approximated by the tabulated values for Ni, whereas for Cm the values tabulated for U were used. No corrections were made for the energy straggling, which occurs upon passage of the projectiles through the Havar window, the nitrogen cooling gas, and the Be target backing.

In order to ensure that all target-like reaction products were collected, a detailed calculation of the involved reaction parameters was performed. First, the probability of a reaction product recoiling from the circular target area hitting the catcher foil must be considered. This problem has been treated in Ref. [16] and only the results of these calculations will be discussed here. The probability of a product nucleus hitting the catcher foil in this target arrangement is 1 if it is emitted between 0° and 51° to the beam axes. The probability then decreases monotonically to 0 between 51° and 71°. Secondly, the grazing angles in the laboratory system of projectile-like and target-like reaction products have to be calculated. This was done using the "sharp cutoff" approximation [34], assuming a grazing collision with no mass transfer and a loss of total kinetic energy (TKE) of 10 MeV throughout the interaction. A summary of calculated reaction parameters for the investigated systems is provided in Table I. With increasing bombarding energy the target-like reaction products are emitted closer to the acceptance angle of the target arrangement; however, even at the largest calculated emission angle of 54°, the probability of a recoiling target-like nucleus hitting the catcher foil is still 0.95. Thus, all reaction products emerging from quasi-elastic interactions with a small net transfer of nucleons and a small loss of TKE are collected with near 100% efficiency. The collection efficiency for deeply inelastic reaction products, which involve large transfers of nucleons and finite interaction times, has to be considered more thoroughly. If the reacting nuclei stick together and rotate for a certain interaction time, the scattering angle $\theta_{\text{c.m.}}$ decreases and the fragments no longer recoil at the calculated grazing angles. Projectile-like fragments are emitted at laboratory angles $\delta_{P\,\text{lab}}$ smaller than the calculated grazing angle, whereas the target-like reaction products recoil at angles $\Omega_{T\,\text{lab}}$ larger than the calculated grazing angle and are eventually lost due to the kinematic limitations of our target arrangement. The scattering angle also depends on the net number of nucleons transferred, the transfer direction, and the TKE loss throughout the interaction. Our calculations indi-

TABLE I. Summary of reaction parameters for the interactions of ^{40}Ca, ^{44}Ca, and ^{48}Ca projectiles with ^{248}Cm.

Projectile	E_{lab}[a] (MeV)	$E_{\text{c.m.}}$[b] (MeV)	$E_{\text{c.m.}}/E_{\text{Coul}}$[c]	$\theta_{\frac{1}{4}\text{c.m.}}$[d] (deg)	$\Omega_{T\,\text{lab}}$[e] (deg)	$\delta_{P\,\text{lab}}$[e] (deg)
^{40}Ca	230.0–235.5	198.1–202.8	0.98–1.00	173	3	172
^{40}Ca	251.5–256.8	216.6–221.1	1.07–1.09	119	30	110
^{40}Ca	286.2–291.3	246.6–250.8	1.22–1.24	87	46	78
^{44}Ca	230.8–236.5	196.0–200.9	0.98–1.00	178	1	177
^{44}Ca	251.2–256.7	213.3–218.0	1.06–1.09	121	29	111
^{44}Ca	273.6–279.0	232.4–237.0	1.16–1.18	97	41	86
^{44}Ca	284.7–290.5	241.8–246.7	1.20–1.23	89	45	78
^{44}Ca	295.9–301.1	251.3–255.7	1.25–1.27	82	48	72
^{44}Ca	318.0–323.1	270.1–274.4	1.34–1.37	71	54	62
^{48}Ca	223.0–239.0	186.8–200.2	0.94–1.01	164	8	160
^{48}Ca	247.0–263.0	206.9–220.4	1.04–1.11	122	29	111
^{48}Ca	272.0–288.0	227.9–241.3	1.15–1.21	95	42	84
^{48}Ca	304.0–318.0	254.7–266.4	1.28–1.34	76	51	66

[a]The energy range of the beam in the target material in the laboratory system, E_{lab} (MeV). Energies for ^{48}Ca from Ref. [6].

[b]The energy range of the beam in the center-of-mass system, $E_{\text{c.m.}}$ (MeV).

[c]The ratio of c.m. energy and interaction barrier, $E_{\text{c.m.}}/E_{\text{Coul}}$, $E_{\text{Coul}}=Z_1Z_2e^2/R_{\text{int}}$ (MeV), $R_{\text{int}}=C_T+C_P+4.49-(C_T+C_P)/6.35$ (fm) (Ref. [49]), where C_T and C_P are the matter half-density radii of the target and the projectile, respectively. $E_{\text{Coul}}=202.3$, 200.6, and 198.9 MeV for interactions with ^{40}Ca, ^{44}Ca, and ^{48}Ca projectiles with ^{248}Cm, respectively.

[d]The calculated quarter point angle in the c.m. system, $\theta_{1/4\text{c.m.}}$ (deg), $\theta_{1/4\text{c.m.}}=2\arcsin[n\lambda\!\!\!^{-}/(R_{\text{int}}-n\lambda\!\!\!^{-})]$ where n represents the Sommerfeld parameter and $\lambda\!\!\!^{-}$ the de Broglie wavelength.

[e]The calculated grazing scattering angles in the laboratory system for the target-like and the projectile-like fragment, respectively, assuming no mass transfer and a kinetic energy loss of 10 MeV during the interaction, $\Omega_{T\,\text{lab}}$, $\delta_{P\,\text{lab}}$ (deg).

cate that all above-target reaction products are still collected with near 100% efficiency. However, with increasing bombarding energies considerable losses of below-target reaction products, such as ^{230}U and ^{227}Th, corresponding to transfers of 18 and 21 nucleons, respectively, cannot be excluded. It was not possible to account for these losses. For the cross-section calculations, we assumed that all detected reaction products were collected with 100% efficiency, which is a valid assumption for reaction products heavier than the target nucleus, and reaction products emerging from quasielastic interactions at near barrier energies.

B. Chemical separations

The chemical separation procedure yielding fractions of individual actinide elements suitable for the determination of gamma and/or alpha and spontaneous fission (SF) activities had to meet several requirements. In order to save beam time, a simple and fast procedure was required that separates all elements of interest. Furthermore, high decontamination factors for individual elements are required since actinide products are formed in small yields in heavy ion transfer reactions. Production cross sections range from several nanobarns to a few millibarns only. Large quantities of unwanted activities are due to reactions of the projectiles with components of the target chamber, i.e., N_2, Be, O (in Cm_2O_3), and Cu (catcher foil). Interfering activities also originate from prompt fission of target-like reaction products. In an attempt to determine relatively short-lived products below the target in the reactions of ^{40}Ca+^{248}Cm, the fast separation procedure outlined in Ref. [35] was applied. The production cross sections for the above-target nuclides formed in these reactions have been measured previously [6]. In the experiments with ^{44}Ca projectiles, the separation procedures for below-target elements described in Ref. [35] were modified and combined with separation procedures for the above-target elements [36] in order to measure production cross sections for all elements from Ra through Md from the same irradiation. The irradiated Cu catcher foils (up to 50 mg) were dissolved in concentrated HNO_3 containing traces of $HClO_4$ and yield tracers of ^{241}Am, ^{239}Pu, and ^{237}Np in equilibrium with ^{233}Pa, ^{233}U, and ^{229}Th in equilibrium with their daughters. The chemical yield of the heavy actinides Bk through Fm was determined by the addition of ^{170}Tm tracer before the element separation. The detailed separation procedure is given in Ref. [37].

The chemically separated fractions containing elements Bk through Am, and Pu/Np were coprecipitated with LaF_3, filtered, and assayed by gamma-ray spectroscopy. Fractions of Pa, Th, and U were gamma counted as liquids in small vials. Elements U and Th were later electrodeposited [38] on platinum disks for alpha spectroscopy. The fractions of Cf, Es, and Fm were each dried on platinum disks and assayed by gamma-ray spectroscopy as well as by alpha spectroscopy and SF counting.

When four to six experimenters cooperated on the separation, purification, and preparation of the samples, the complete procedure required 3.5 h from the end of the bombardment (EOB) until the start of the measurement of the last sample. The first samples containing relatively short-lived nuclides were separated and prepared for counting in about 30 min after EOB. Chemical yields as determined with yield tracers ranged from 40% to 95%.

C. Data acquisition and analysis

The various fractions were counted for gamma-ray activities, each with one of five Ge(Li) or high purity Ge detectors. Alpha-particle and SF activities were detected using Si(Au) surface barrier detectors.

Gamma-ray spectra were analyzed using the SAMPO [39] or the NEWFIT [40] code. Very small peaks, that were not identified by the automatic peak search routine, were integrated by summing the peak channels and subtracting a linear background. Complex alpha spectra were analyzed with the NEWFIT [40] code, which uses tabulated alpha-branching ratios. Very small peaks with only a few counts were integrated by summing the appropriate channels.

Decay-curve analyses were performed with the EXFIT [41] code, which yielded the activities at EOB. Half-lives from Ref. [32] were used. In the case of growth and decay, the initial activity of the daughter was fixed at zero at the time when a separation of mother and daughter products was performed. Since the production cross sections for below-target elements were small in the experiments with ^{40,44}Ca projectiles, some nuclides could not be detected. For these cases upper activity limits were estimated with the method of Ref. [42]. The activities at EOB were corrected for the detector efficiency, the abundance of the specific radiation, and the chemical yield. Production cross sections were calculated using the activities at EOB corrected for decay during the irradiation, the nuclide half-lives, and the target thickness and the irradiation history. A 100% collection efficiency for transfer products was assumed for all experiments. The following statistical errors have been included in the cross section calculations: (i) errors in the initial activities after EOB resulting from the decay curve analysis, (ii) errors in the detector efficiency function, (iii) errors in the chemical yields, and (iv) errors in determining the target thickness, which were assumed to be 5%. Errors in the quoted half-lives and radiation abundances were neglected. No error was included for the electrometer readings of the beam intensity. All errors were treated and propagated as standard deviations (1σ) to give the total errors of the cross sections.

III. RESULTS

The cross sections ($d\sigma^2/dZ\,dN$) measured in this work and in Ref. [30] for the production of below-target elements ($Z_{\text{prod}} \leq Z_{\text{target}}$) in the reactions of ^{40}Ca ions with ^{248}Cm at three different bombarding energies are given in Table II. The results of our measurements for bombardments of ^{248}Cm with ^{44}Ca projectiles are given in Tables III and IV, respectively. Table III summarizes the measured cross sections for isotopes of below-target elements ($Z_{\text{prod}} \leq Z_{\text{target}}$) Th, U, Np, Pu, Am, and Cm at four different energies, whereas the measured production cross

sections for isotopes of the above-target elements ($Z_{prod} > Z_{target}$) Bk, Cf, Es, and Fm are given in Table IV.

In order to allow a comparison of the actinide yields from the reactions of $^{40,44,48}Ca+^{248}Cm$, Fig. 1 summarizes all existing data from this work and other studies [6,9,30] at an interaction energy corresponding to about $1.1E_{Coul}$. At this bombarding energy the most complete set of data exists. The shapes of almost all above-target isotope distributions in the reactions of $^{40,44,48}Ca+^{248}Cm$ are quite similar and can be represented by Gaussian distributions with a full width at half maximum (FWHM) of ≈ 2.5 mass numbers. The distribution of the Fm isotopes in the experiment with ^{44}Ca appears to be asymmetric. The decay of ^{256}Md contributes to ^{256}Fm since ^{256}Md decays 90.7% by electron capture. Assuming that all ^{256}Fm is due to the decay of ^{256}Md, an upper production cross section limit of ^{256}Md can be estimated at 0.2 μb. The FWHM's of below-target isotopic distributions in the reactions of $^{48}Ca+^{248}Cm$ have been determined by Gäggeler *et al.* [9]. They reported a FWHM of ≈ 5 mass numbers for the distributions of Pu and U isotopes and slightly broader distributions with FWHM ≈ 5.5 mass numbers for Th, Ac, Ra, and Rn. Even though the data for below-target elements are rather fragmentary in the experiments with ^{44}Ca, and especially with ^{40}Ca projectiles, FWHM of ≈ 5 mass numbers and ≈ 5.5 mass numbers, respectively, also seem to apply. The isotopic distributions for elements with fragmentary or no measured data have been reconstructed using further assumptions that will be discussed in Sec. IV. The cross section of

TABLE II. Cross sections for the production of actinides with $Z_{prod} \leq Z_{target}$ in bombardments of ^{248}Cm with ^{40}Ca projectiles of different energies.

Nuclide		230.0–235.5 MeV		251.5–256.8 MeV		286.2–291.3 MeV	
		Cross section[a] (μb)	s[b] (%)	Cross section[a] (μb)	s[b] (%)	Cross section[a] (μb)	s[b] (%)
Cm	249	< 130		< 148		696	44
Am	247	< 55.6		< 49.5		< 77.4	
	246*m*	< 48.3		< 40.3		< 55.3	
	246*g*	< 8.3		10.0	15	29.9	12
	245	32.2	48	73.9	24	135	17
	244*g*	10.7	16	25.6	9	49.9	11
	240	< 3.8		12.7	12	14.8	47
	239	–		< 7.2		< 15.7	
Pu	246	< 16.8		< 23.1		< 86.6	
	245	< 11.8		< 16.5		< 37.3	
	243	< 6.6		< 8.4		< 17.5	
	236[c]	–		0.87	67	0.34	35
Np	240*g*	< 17.9		< 17.9		< 30.5	
	239	< 5.4		< 7.0		< 16.1	
	238	< 13.1		< 18.2		< 45.9	
	234	< 21.1		< 26.1		< 106	
U	240	< 18.7		< 31.0		< 22.3	
	239	< 18.4		< 28.8		< 13.3	
	237	< 5.5		< 6.1		< 10.8	
	230[c]	0.11	18	0.34	38	0.013	15
Pa	234*g*	< 32.9		< 23.4		< 40.6	
	232	< 38.5		< 29.8		< 51.0	
	230	< 77.8		< 93.8		< 214	
	228	< 84.2		< 70.5		< 130	
Th	228[c]	4.3	35	16.0	25	2.1	24
	227[c]	0.36	31	0.26	42	0.25	40

[a]Detection limits are indicated with <.

[b]Standard deviation (1σ). The calculation of the errors is described in the text.

[c]Data from Ref. [30] measured with a thicker ^{248}Cm target. The energies incident on target in Ref. [30] were 221–234, 246–259, and 281–294 MeV, for Pu, U, and Th, respectively. The cross section for ^{228}Th is partly due to ^{228}Pa, since the irradiated catcher foil was not processed immediately after the bombardment.

TABLE III. Cross sections for the production of actinides with $Z_{prod} \leq Z_{target}$ in bombardments of ^{248}Cm with ^{44}Ca projectiles of different energies.

Nuclide		230.8–236.5 MeV		251.2–256.7 MeV		284.7–290.5 MeV		318.0–323.1 MeV	
		Cross section[a]	s[b]	Cross section[a]	s[b]	Cross section[a]	s[b]	Cross section[a]	s[b]
		(μb)	(%)	(μb)	(%)	(μb)	(%)	(μb)	(%)
Cm	249	772	15	2850	22	4710	18	5410	38
Am	247	<102		264	52	994	15	1430	37
	246*m*	<67.9		256	25	507[c]	19	<1135	
	246*g*	<9.7		67.0	15	152	10	210	24
	245	86.3	19	294[d]	13	512[d]	17	544[d]	25
	244*g*	31.4	8	117	8	183	7	173	10
	240	9.3	31	29.4	28	21.0	27	25.4	29
	239	<3.1		<11.2		9.6	25	<9.4	
Pu	246	<5.1		<11.9		7.4	40	22.2	35
	245	<1.9		7.7	25	12.7	20	32.9	36
	243	12.7	31	19.1	19	40.8	10	56.7	11
	236	<0.22		<2.2		<4.0		<8.4	
Np	240*g*	–		<66.1		<21.6		<252	
	239	<14.2		10.5	20	11.5	29	<184	
	238	<48.3		<18.8		<21.6		<209	
	234	<114		<41.9		<27.1		<139	
U	237	1.0	72	3.5	31	4.0	26	6.6	74
	230	0.28	15	0.79	22	<0.27		<0.22	
Th	227	9.3	18	6.9	24	2.3	19		

[a]Detection limits are indicated with <.
[b]Standard deviation (1σ). The calculation of the errors is described in the text.
[c]Corrected for contribution of ^{246}Pu parent.
[d]Corrected for contribution of ^{245}Pu parent.

^{228}Th(^{228}Pa) determined in the reactions of ^{40}Ca+^{248}Cm (Ref. [30]) appears to be too high to be consistent with the measured cross sections for the nuclides ^{227}Th and ^{230}U.

At the same bombarding energy above the Coulomb barrier, the yield of below-target elements is about one order of magnitude higher in the reactions with ^{48}Ca projectiles compared to ^{44}Ca projectiles and about two orders of magnitude higher compared to ^{40}Ca projectiles. Differences also exist in the yields of above-target elements, but they are far less pronounced than for the below-target products. The yield of Fm is about five times higher in the reactions with ^{44}Ca projectiles compared to ^{40}Ca projectiles and about one order of magnitude higher compared to ^{48}Ca projectiles.

IV. DISCUSSION

The observed mass distributions in heavy ion reactions are secondary distributions. They differ from the primary ones due to deexcitation by either particle emission, mostly neutrons, or, in the case of very heavy fragments, by particle emission and/or sequential fission. These fast processes prevent the detection of primary reaction products. The reconstruction of the primary reaction product distribution from the observed mass distributions, which is essential for the discussion of processes occurring during the interaction, strongly relies on the proton number Z, the neutron to proton ratio N/Z, the excitation energy E^*, and the angular momentum l of the primary fragments.

In order to compare the results of previous reaction studies [6,9,30] with the present work, the rather incomplete data, especially in experiments with ^{40}Ca, have to be supplemented by reconstruction of isotopic distributions. This can be done with a knowledge of (i) the FWHM for this type of reaction and (ii) the most probable mass number of the secondary distribution $\langle A' \rangle_Z$. The assignment to a certain type of reaction (quasielastic, deeply inelastic, quasifission) is based mainly on the observed FWHM of the measured secondary mass distribution, which is different [19] for each type of reaction.

Several authors [9,10,14,18–21] have shown that the equilibration of the N/Z ratio is related to the TKE loss and strongly governed by the underlying PES. PES's are therefore useful tools for inferring the most probable mass number of the primary distribution $\langle A \rangle_Z$. In addition to the published PES [9] of the system ^{48}Ca+^{248}Cm, PES's for the two other systems ^{40,44}Ca+^{248}Cm have been calculated.

Examination of the measured excitation functions for the reactions of ^{40,44}Ca with ^{248}Cm reveals some informa-

tion about the distribution of excitation energy among the complementary reaction partners and the conversion of excess kinetic energy into internal excitation of the reaction products. The excess energy available for product excitation is estimated on the basis of a model introduced by Hoffman and Hoffman [43,44].

A. FWHM of mass distributions

The widths of secondary isotope distributions in dissipative heavy ion reactions can be deconvoluted [14,45] into three contributions: (i) the primary width; (ii) contributions due to fluctuations in the excitation energy, and the number of evaporated neutrons; and (iii) the intrinsic width of the neutron evaporation process at fixed excitation energy. In addition, the width should also depend on the curvature of the PES. As mentioned above, the secondary isotopic distributions in the reactions of ^{40,44,48}Ca with ^{248}Cm can be represented by Gaussians with FWHM$\approx$2.5 mass numbers. In fact, similar FWHM values ranging from 2 to 3 mass numbers have been reported in experiments with light heavy ions, such as ^{16,18}O and ^{20,22}Ne (Refs. [4,5]), medium weight projectiles such as ^{31}P and ^{40}Ar (Refs. [15–17]), as well as with heavy projectiles like ^{86}Kr, ^{129,132,136}Xe, and ^{238}U (Refs. [3,7,10]). These relatively narrow widths are characteristic for quasielastic transfer reactions with small kinetic energy losses [19] and indicate that the detected nuclides are produced with little excitation energy.

The broader distributions for below-target elements (i.e., FWHM$\approx$5–5.5 mass numbers) indicate that these reactions must be attributed to predominantly inelastic interactions [45] (deeply inelastic and quasifission) with considerable conversion of kinetic energy into excitation of the fragments.

TABLE IV. Cross sections for the production of actinides with $Z_{prod} > Z_{target}$ in bombardments of ^{248}Cm with ^{44}Ca projectiles of different energies.

Nuclide		230.8–236.5 MeV		251.2–256.7 MeV		273.6–279.0 MeV		295.9–301.1 MeV		318.0–323.1 MeV	
		Cross section[a] (μb)	s[b] (%)	Cross section[a] (μb)	s[b] (%)	Cross section[a] (μb)	s[b] (%)	Cross section[a] (μb)	s[b] (%)	Cross section[a] (μb)	s[b] (%)
Bk	244[c]	8.1	9	18.7	17	27.2	6	29.0	15	21.2	16
	245	116	8	315	6	391	11	503	7	322	14
	246	380	8	870	10	1220	4	1360	12	972	25
	248*m*	1000	7	2080	17	2990	14	3350	27	2710	25
	250	153	6	513	6	858	7	1050	10	1380	7
	251	< 28.3		< 94.3		–		–		6.6	74
Cf	246	41.5	5	113	8	131	7	126	10	19.3	10
	247	168	10	254	18	330	20	250	18	< 142	
	248[d]	580	8	1630	7	2380	5	1808	8	647	14
	250[e]	1690	28	7040	9	5490	4	5340	5	5500	8
	252[f]	368	24	856	10	1710	10	1410	12	231	10
	253	1.2	14	5.1	11	8.5	11	7.6	20	1.1	28
Es	249	34.4	10	49.1	13	38.0	5	–		–	
	250*g*	26.5	5	35.2	8	32.0	17	28.5	9	9.1	14
	250*m*	43.7	25	87.3	22	176	25	122	26	< 48.4	
	251	52.4	26	127	22	250	10	160	18	41.6	27
	252	18.4	15	45.3	13	118	21	69.9	24	15.3	34
	253[g]	10.3	11	9.9	10	9.2	14	12.0	15	2.1	13
	254*m*	0.27	20	0.66	17	0.86	12	0.74	15	0.15	15
Fm	250	< 0.46		< 3.9		–		< 19.5		< 5.9	
	252[h]	8.1	8	20.9	8	13.9	9	7.9	6	3.6	25
	253	3.3	16	13.0	12	13.2	9	6.2	6	1.2	14
	254[i]	1.5	11	4.5	9	3.3	3	1.4	14	0.26	20
	256	0.19	15	0.34	30	0.18	10	0.11	8	0.04	40

[a]Detection limits are indicated with <.
[b]Standard deviation (1σ). The calculation of the errors is described in the text.
[c]An intensity of 100% was assumed for the measured 891.5-keV gamma ray of ^{244}Bk.
[d]Corrected for contribution from decay of ^{248}Bk^{m}, and ^{252}Fm parent.
[e]Corrected for contribution from decay of ^{250}Bk, ^{250}Es^{m}, ^{250}Es^{g}, and ^{254}Fm parent.
[f]Corrected for contribution from decay of ^{252}Es parent.
[g]Corrected for contribution from decay of ^{253}Cf parent.
[h]All activity observed from 7.0-MeV α particles in the Fm fraction was assigned to ^{252}Fm.
[i]Corrected for contribution from decay of ^{254}Es^{m} parent.

B. Potential energy surface calculations

The average drift of the heavy fragment charge and mass distributions away from the initial charge and mass of the target nucleus is strongly influenced by the local gradient $[(\Delta E_p/\Delta Z)^2+(\Delta E_p/\Delta N)^2]^{1/2}$ in the underlying PES [9,10,14,18–21]. On the basis of PES calculations the most probable mass $\langle A \rangle_Z$ of the isotopic distributions can be predicted. Gross *et al.* [31] predict $\langle A \rangle_Z$ at the configuration for which the density of levels is highest in the dinuclear complex. This configuration corresponds to the highest excitation energy and to a minimum in the potential energy (PE) of the system [31]. The PE of a given product pair, E_{prod}, is given by the Coulomb (E_{Coul}), nuclear (E_{nucl}), and centrifugal (E_{cent}) potentials evaluated at its interaction radius:

$$E_{\text{prod}}=E_{\text{Coul}}+E_{\text{nucl}}+E_{\text{cent}} \ . \tag{1}$$

The mathematical forms of the Coulomb, nuclear, and centrifugal potentials used are from Ref. [46]. A phenomenological Coulomb potential was developed by Bondorf *et al.* [47]; the nuclear potential used is a proximity potential [48]. The interaction radius R_{int} was calculated for each product pair according to a semiempirical formula by Wilcke *et al.* [49], which has been derived from a fit to a compilation of experimental R_{int} values. The PES is a plot constructed from the differences in PE (ΔE_p) between specific product pairs and the reactants (E_{react}), evaluated at their respective interaction radii, minus the ground state Q value (Q_{gg}) for that reaction:

$$\Delta E_p=E_{\text{prod}}-E_{\text{react}}-Q_{gg} \ . \tag{2}$$

The computer code HEAVI [10] was used to calculate PES's, neglecting angular momentum effects ($l=0\hbar$). The masses used in the calculation of the PES were Myers-Swiatecki liquid droplet masses [50] with shell corrections. The even-odd term in the liquid droplet masses was neglected in order to give a smoother PES contour map representation. The calculated liquid droplet masses of actinide nuclides are often 1.0–1.5 MeV less than the actual ground state masses [32]; therefore, the computer code HEAVI [10] includes corrections for liquid droplet actinide masses, based on the actual ground state masses. Since the liquid droplet model is unable to accurately predict the masses of very light nuclei, actual ground state masses (where available) were incorporated into the code for nuclei with Z or $N<10$. No frictional forces or nuclear deformations occurring during the interaction are considered and incorporated in the code.

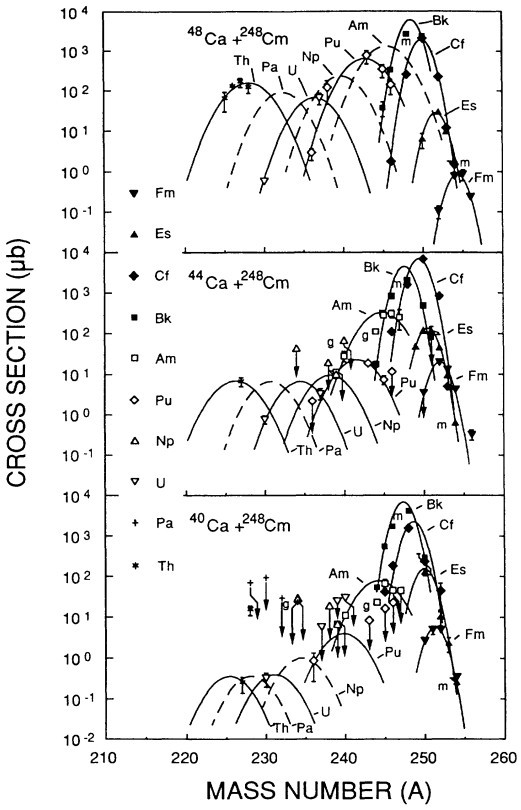

FIG. 1. Isotopic distributions of actinides in reactions of Ca isotopes with ^{248}Cm. Ground state isomers or metastable isomers are denoted with "g" or "m", respectively. Arrows indicate detection limits. Top: Reactions of 247–263-MeV ^{48}Ca projectiles with ^{248}Cm (Refs. [6,9]). Middle: Reactions of 251.2–256.7-MeV ^{44}Ca projectiles with ^{248}Cm (this work). Bottom: Reactions of 251.5–256.8-MeV ^{40}Ca projectiles with ^{248}Cm. The data of Ref. [6] (above-target nuclides) and the data of Lerch *et al.* (Ref. [30]) (^{227,228}Th, ^{230}U, and ^{236}Pu) are from reactions of 246–259-MeV ^{40}Ca.

In Fig. 2 the PES's of the three systems ^{48}Ca+^{248}Cm, ^{44}Ca+^{248}Cm, and ^{40}Ca+^{248}Cm are represented by contour maps. As already shown by Gäggeler *et al.* [9] the maxima of the mass distributions in experiments with ^{48}Ca closely follow the bottom of the PES valley. The injection point is located close to N/Z equilibrium and there is no strong local gradient that would indicate an energetically preferred transfer direction. The evolution of the system towards fusion is energetically hindered at the Coulomb barrier, since the Businaro-Gallone saddle point [51] at $Z=106$ and $N=166$ is at $+15.7$ MeV. The development of the interaction towards symmetry is therefore favored. The fact that the maxima of the mass distributions $\langle A' \rangle_Z$ of the elements Rn through Fm are close to N/Z equilibrium indicates that these nuclides are produced with very little excitation energy [9]. This leads to the conclusion that the primary mass distributions of the elements Rn through Fm are only slightly or not altered by neutron evaporation processes. However, a deexcitation of primary reaction products by sequential fission cannot be excluded. Maxima of mass distributions that have not been measured were interpolated on the basis of the existing data, the calculated minimum of the PES and FWHM of the Gaussian mass distributions.

In the experiments with ^{44}Ca, the ^{248}Cm injection point is displaced by ≈ 4 mass numbers to the neutron-rich side compared to N/Z equilibrium. A strong local gradient of 4.8 MeV/mass number favors the production of ^{248}Bk. Then the energetically most favorable drift direction points to ^{247}Bk and from there to ^{244}Am towards symme-

try. The evolution of the system towards compound nucleus formation is energetically slightly hindered at the Coulomb barrier; the saddle point of this system at $Z=106$ and $N=162$ is $+4.7$ MeV. A transfer of 4 protons from the projectile to the target nucleus is needed to reach the line of N/Z equilibrium for the above-target products. The same number of protons and about 16 neutrons need to be transferred from the target nucleus to the projectile to reach the line of N/Z equilibrium for below-target products. The maxima of the experimentally determined distributions are located on the neutron-rich side of the N/Z equilibrium minimum of the PES valley. This result can be interpreted as follows: Starting with quasielastic transfer reactions about 4 protons are transferred to reach the region of the N/Z-equilibrated, deeply inelastic interactions in either direction. All the maxima of the transcurium elements are located near the $N=152$ closed neutron shell of the target nucleus, which might account for this effect. The maxima of the below-target isotope distributions are displaced between 3 and 4 mass units towards lower neutron numbers with each proton transferred from the target nucleus to the projectile. Maxima which were not measured have been interpolated.

With the ^{40}Ca projectile, the injection point falls on a very steep gradient of the PES. The injection point is displaced by 8 mass numbers to the neutron-rich side of the PES. A very strong local gradient of 8.9 MeV/mass

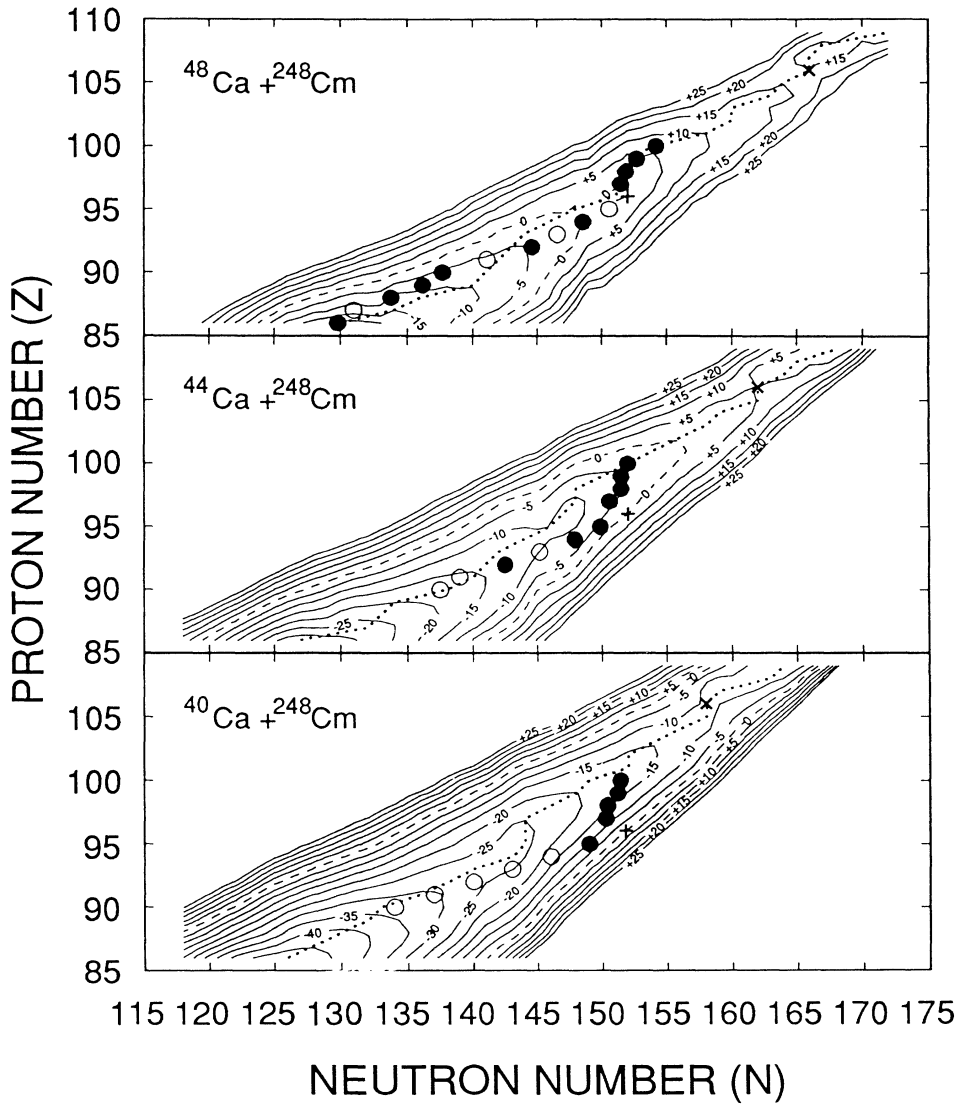

FIG. 2. Contour map representation of the calculated PES for the reactions of ^{40,44,48}Ca projectiles with ^{248}Cm at an angular momentum of $l=0\hbar$. The dashed lines denote the equipotential contour lines at 0 MeV. The injection points (^{248}Cm) are represented by $+$. The dotted lines connect the minima of the potential energies calculated for each Z. The Businaro-Gallone saddle point is indicated by $\times$. The filled circles represent the position of the experimentally determined maxima of the isotopic distributions for each Z, whereas the open circles represent the estimated maxima. ^{48}Ca data from Refs. [6,9] and ^{40}Ca data partly from Refs. [6,30].

number points towards the production of ^{248}Bk. The energetically most favorable drift direction continues, still with a strong gradient of 4.9 MeV/mass number, to ^{248}Cf and ^{248}Es before it turns around towards symmetry. The evolution towards compound nucleus formation is energetically no longer hindred at the barrier; the saddle point at $Z=106$ and $N=158$ now is at -10.6 MeV. Similar to the ^{44}Ca+^{248}Cm system, a transfer of about 4–5 protons is needed to reach N/Z equilibrium for above-target elements. For below-target elements only the maximum of the Am isotope distribution was determined. The maxima of the missing below-target elements have been estimated assuming that as in the ^{44}Ca+^{248}Cm system about 4–5 protons are transferred in either direction to reach N/Z equilibrium. This results in a displacement of the maxima of about 4 mass numbers towards smaller neutron numbers with each proton transferred from the target to the projectile. The calculated most probable mass numbers $\langle A \rangle_Z$, the experimentally determined and the estimated maxima of the secondary distributions $\langle A' \rangle_Z$, are summarized in Table V.

The different neutron numbers of ^{40}Ca, ^{44}Ca, and ^{48}Ca are only partly reflected in the target-like products. The differences between the positions of the maxima of the mass-yield curves for Bk, Cf, and Es are smaller than 1 mass number between the reactions of ^{40}Ca and ^{44}Ca, and about 1–2 mass numbers between those of ^{40}Ca and ^{48}Ca. The maxima of the Fm mass-yield curves differ by less than 1 mass number between the ^{40}Ca and ^{44}Ca reactions, but by about 3 mass numbers between those of ^{40}Ca and ^{48}Ca. This may be due to the particular shapes of the N/Z-equilibrium lines, which are similar in all three systems. In the reactions with ^{44}Ca and ^{40}Ca this line is displaced by about 4 and 8 mass numbers towards lower neutron numbers, respectively, compared to the reactions with ^{48}Ca. In the reactions with ^{48}Ca the maxima of the above-target mass distributions closely follow this line, which results in neutron-rich Es and Fm isotopes. In the case of the ^{44}Ca and ^{40}Ca projectiles, where the N/Z-equilibrium line is achieved only after the transfer of 4 to 5 protons, the displacement of the isotopic distributions toward neutron-rich reaction products should become noticeable for the transfermium isotopic distributions. It is very remarkable that the equilibration of the N/Z ratio for above-target products gradually occurs by the transfer of protons and not by neutrons which would result in a strong shift of the maxima of the mass distributions towards the line of N/Z equilibrium. The transfer of protons to the target nucleus seems to be the dominant reaction path in the reactions of ^{40}Ca and ^{44}Ca whereas with ^{48}Ca the system shows no preferential transfer direction.

The maxima of the isotopic distributions of the below-target elements differ by no more than 2–4 mass numbers between the three different projectiles, due to the fact that N/Z equilibrium is only gradually approached by the transfer of 4 or more protons in the case of ^{40}Ca and ^{44}Ca.

C. Calculated excitation energies

In a radiochemical experiment with one thick catcher foil all information about the kinetic energy of the fragments is lost. Thus, assumptions have to be made about the conversion of excess kinetic energy into internal excitation energy, the deformation of the fragments in the exit channel, and the partition of the excitation energy among the fragments.

TABLE V. Calculated most probable primary mass numbers $\langle A \rangle_Z$ in the PES and measured maxima of the secondary mass distributions $\langle A' \rangle_Z$ in the reactions of ^{40,44,48}Ca projectiles with ^{248}Cm at bombarding energies corresponding to $1.1E_{\text{Coul}}$.

Element	Projectile ^{40}Ca[a]		^{44}Ca		^{48}Ca[b]	
Z	$\langle A \rangle_Z$	$\langle A' \rangle_Z$	$\langle A \rangle_Z$	$\langle A' \rangle_Z$	$\langle A \rangle_Z$	$\langle A' \rangle_Z$
100	249.0	251.4	252.0	252.0	254.0	254.2
99	247.0	250.2	249.0	250.5	251.0	251.7
98	244.0	248.4	246.0	249.5	250.0	249.9
97	241.0	247.3	245.0	247.6	249.0	248.5
96	240.0		243.0		247.0	
95	239.0	244.0	241.0	244.9	243.0	245.6[c]
94	237.0	240.0[c]	238.0	241.9	240.0	242.6
93	233.0	236.0[c]	235.0	238.2[c]	237.0	239.6[c]
92	230.0	232.0[c]	233.0	234.5	235.0	236.6[c]
91	227.0	228.0[c]	231.0	230.0[c]	233.0	232.1[c]
90	223.0	224.0[c]	228.0	227.5[c]	231.0	227.7
89	221.0		223.0		229.0	225.2
88	218.0		221.0		224.0	221.8
87	215.0		219.0		221.0	218.0[c]
86	212.0		213.0		216.0	215.8

[a]Based on data from Refs. [6,30] and this work.
[b]Based on data from Refs. [6] and [9].
[c]Estimated $\langle A' \rangle_Z$.

1. Excess energy available for product excitation

Two limiting cases, namely, touching spheres and deformed nuclei, will be discussed in the following.

a. Touching spheres. Under the assumption that the primary fragments reseparate as touching spheres, the excess energy available for product excitation, E^*, is related to ΔE_p by

$$E^* = E_{K,\text{in}} - E_{K,\text{out}} - \Delta E_p \ , \tag{3}$$

where $E_{K,\text{in}}$ and $E_{K,\text{out}}$ are the residual kinetic energies of the reactants and the products in the c.m. frame, respectively, before and after the nucleon transfer process has occurred. In the present calculations, it was assumed that the kinetic energy converted into internal excitation is proportional to the number of nucleons exchanged [43]. The entries in Table VI are solutions of the equation

$$E^* = (E_{\text{c.m.}} - E_{\text{react}}) \frac{N_{\text{ex}}}{A_{\text{Ca}}} - \Delta E_p \ , \tag{4}$$

where $E_{\text{c.m.}}$ is the kinetic energy in the c.m. system, A_{Ca} is the mass of the projectile, and N_{ex} is the number of protons and neutrons exchanged. Again, the code HEAVI [10] was used to compute excitation energies. Contrary to the PES calculations, the calculated excitation energies are very sensitive to the Coulomb potential and the interaction radius. As in the PES calculations, the semiempirical radius R_{int} of Ref. [49] was used.

The comparison (Table VI) of the calculated excitation energies in the three systems ^{40,44,48}Ca+^{248}Cm at an energy of $1.1E_{\text{Coul}}$ shows that the lowest excitation energies result for the reactions with ^{48}Ca and the highest for the interactions with ^{40}Ca. The calculations for ^{40}Ca lead to excitation energies of the above-target nuclides of up to 29 MeV and up to 47 MeV for the below-target nuclides. Depending on the division of the excitation energy among the fragments, such high excitation energies may lead to considerable losses of target-like fragments due to sequential fission and/or neutron emission. The problem of how the excitation energy is distributed between the fragments will be addressed later in this section.

In the reactions of ^{44}Ca+^{248}Cm the formation of above-target nuclides results in calculated excitation energies that are positive by 6–12 MeV for most of the observed products; this may favor the production of above-target nuclides, without introducing too much excitation energy. The formation of below-target products results in maximum calculated excitation energies of the fragments between 14 and 28 MeV depending on the Z and A of the product nuclei. The calculated excitation energies are about 10 MeV higher than those from interactions of ^{48}Ca+^{248}Cm.

In the system ^{48}Ca+^{248}Cm, reactions leading to above-target nuclides result in calculated excitation energies between 1 and −4 MeV. Negative excitation energies mean that in the frame of this model a higher injection energy than $1.1E_{\text{Coul}}$ would be needed to form these nuclides. The excitation energies for the formation of below-target nuclides are positive by 1–16 MeV. This indicates that all products are formed essentially cold. This finding agrees well with the conclusions from the PES calculations. The considerable differences in the calculated excitation energies between the three systems ^{40,44,48}Ca+^{248}Cm are mostly due to the differences in the Q_{gg} values.

b. Deformed nuclei. Prolate deformations of the nuclei and neck formation may considerably increase the energy available for product excitation. Töke *et al.* [27] have shown that the average kinetic energy release in quasifission reactions for symmetric mass divisions obeys similar systematics as determined by Viola [52] for the average kinetic energy release in fission. The average kinetic energy release in symmetric quasifission reactions [27], $\langle E^*_{\text{fiss}} \rangle_{\text{sym}}$, follows the expression

$$\langle E^*_{\text{fiss}} \rangle_{\text{sym}} = 0.1240 \frac{Z^2}{A^{1/3}} \ , \tag{5}$$

where Z is the proton number and A is the mass of the

TABLE VI. Calculated excitation energies available for product exitation in the reactions of ^{40}Ca, ^{44}Ca, and ^{48}Ca+^{248}Cm at bombarding energies of $1.1E_{\text{Coul}}$. The calculation of E^* and E^*_{fiss} is described in the text [Eqs. (4) and (6)].

	Projectile								
	^{40}Ca			^{44}Ca			^{48}Ca		
Element[a] Z	$\langle A \rangle_Z$	E^* (MeV)	$\langle E^*_{\text{fiss}} \rangle_{\text{asym}}$ (MeV)	$\langle A \rangle_Z$	E^* (MeV)	$\langle E^*_{\text{fiss}} \rangle_{\text{asym}}$ (MeV)	$\langle A \rangle_Z$	E^* (MeV)	$\langle E^*_{\text{fiss}} \rangle_{\text{asym}}$ (MeV)
100	249	19	76	252	6	63	254	−4	54
99	247	21	79	249	7	64	251	−2	56
98	244	25	86	246	10	71	250	0	63
97	241	29	89	245	12	73	249	1	64
96	240	32	95	243	14	75	247	1	66
95	239	32	94	241	14	77	243	3	66
94	237	33	96	238	17	81	240	5	71
93	233	35	97	235	20	80	237	8	71
92	230	39	102	233	22	83	235	11	74
91	227	42	102	231	25	86	233	13	78
90	223	47	107	228	28	92	231	16	82

[a] $Z > 96$: above-target elements, $Z < 96$: below-target elements.

compound nucleus. The average kinetic energy release in asymmetric quasifission reactions, $\langle E^*_{\rm fiss}\rangle_{\rm asym}$, can be calculated by scaling $\langle E^*_{\rm fiss}\rangle_{\rm sym}$ proportional to the ratio of the Coulomb energies for asymmetric ($E_{\rm Coul\,asym}$) and symmetric ($E_{\rm Coul\,sym}$) mass and charge divisions:

$$\langle E^*_{\rm fiss}\rangle_{\rm asym}=E_{\rm c.m.}-\langle E^*_{\rm fiss}\rangle_{\rm sym}\frac{E_{\rm Coul\,asym}}{E_{\rm Coul\,sym}}\ . \quad (6)$$

In Table VI the energy available for product excitation including deformations of the fragments in the exit channel was calculated, assuming that all excess kinetic energy was completely converted into internal excitation. The results in Table VI show some 60 to 70 MeV of excitation energies added to the values calculated with the touching spheres model.

2. *Distribution of excitation energy between the fragments*

A problem that has not been discussed so far is the division of excitation energy among the fragments. Usually the excitation energy is divided in damped collisions assuming equal nuclear temperatures in the fragments. In other words, the excitation energy is divided in proportion to the fragment masses. However, several researchers have found that temperature equilibrium is reached only for strongly damped reactions. In the reactions of 8.5 MeV/nucleon ^{56}Fe+^{238}U a temperature equilibrium is not reached up to TKE losses > 100 MeV [53]. For small energy losses the excitation energy is divided almost equally among the heavy and the light fragment ($E^*_h/E^*_l\approx 1$). In the system 8.5 MeV/nucleon ^{74}Ge+^{165}Ho it was found [54] that for the initial phase of the mass drift from the target to the projectile the deposited excitation energy in the projectile is directly proportional to the net number of nucleons transferred. With increasing mass transfer, the one-directional mass flow becomes increasingly randomized, so that an equal share of the total excitation energy is gradually approached. Both systems were investigated at energies well above the Coulomb barrier. In experiments close to the Coulomb barrier, where the two nuclei interact with almost zero relative velocity, the correlation between the division of excitation energy and the net nucleon transfer must be very pronounced.

In the reactions of 248–263 MeV ^{48}Ca+^{248}Cm (Ref. [9]) the authors had to assume either spherical shapes of the fragments or a division of the excitation energy far beyond equipartition to explain the high and constant yields of below-target products. They found a value of $E^*_h/E^*_l\approx 0.2-0.3$. Indeed, very little sequential fission was observed in similar reactions of 5.4 MeV/nucleon ^{48}Ca+^{238}U using detector techniques [27]. An unusual division of excitation energy in quasifission reactions was also observed in the reactions of ^{50}Ti, ^{54}Cr, and ^{58}Fe and ^{207,208}Pb at the Bass-model fusion barrier [28]. Temperature equilibrium was reached only for the most symmetric quasifission reactions. For more asymmetric reactions a division of excitation energy comparable to the value of Ref. [9] was found. Evidently, the transferred nucleons deposit excitation energy in the acceptor and leave the donor unexcited. If the excitation energy remains mainly in the acceptor nucleus, above-target nuclei carry most of the total excitation energy, leaving cold projectile-like fragments. Since the fission barrier heights and the neutron binding energies of heavy actinides are less than 7 MeV, predominantly quasielastic transfer products are observed. Thus, the excitation energies calculated with the model of Ref. [43] should prove valid under the condition that $E^*_h\approx E^*$. Under the assumption that the ratio of $E^*_h/E^*_l\approx 0.2-0.3$ is valid in all three of the investigated systems, the excitation energies E^* in Table VI, calculated for below-target nuclides with the model of Ref. [43], are essentially correct if the heavy fragment carries the total calculated excitation energy, $E^*_h\approx E^*$. The fact that no deformations of the fragments are considered in the model of Ref. [43] nearly compensates for the observed, nonequilibrated excitation energy division in asymmetric quasifission reactions.

D. Excitation functions

Excitations functions of quasielastic transfer reactions are characterized by two main features, (i) a sharp increase of the cross section at incident energies below and at the reaction barrier and (ii) essentially constant yields above the threshold energy [55]. The position of the thresholds of different transfer reactions relative to the calculated Coulomb barrier depends strongly on the reaction energies. Negative reaction energies result in low yields even at projectile energies well above the calculated barrier, whereas positive reaction energies yield significant cross sections below the barrier. The constant yields for above threshold energies indicate that the transfer probability is a maximum for an optimum distance of approach, and that the range of l values, for which the transfer probability is significant, remains constant with increasing incident energies. The essentially flat shape of the excitation functions is, therefore, due to these "geometrical" aspects [55]. The excitation functions measured for actinide products are further modified by deexcitation of primary products by neutron emission and/or fission depending on the neutron binding energies and fission barrier heights of the product nuclei. The identification of a given residual nucleus is generally not sufficient to specify the reaction involved in creating it. For actinide reaction products, excitation functions are expected to show a sharp increase in cross section near the threshold energy, to exhibit a maximum and then a gradual decrease due to fission and/or neutron emission. The maxima of the excitation functions should occur at incident energies which excite the heavy reaction products to the height of the fission barrier or the neutron binding energy, whichever is lower. In Tables VII and VIII the measured and calculated maxima of the excitation functions are compared for the measured isotopes. The model of Ref. [43] was used to calculate the excitation energies which were assumed to excite only the acceptor nucleus, thus, $E^*_h\cong E^*$. Wherever possible, experimental values of fission barrier heights were used [56,57]. Calculated fission barrier heights and neutron binding energies were taken from Ref. [58].

TABLE VII. Energy of experimental and calculated maxima for the excitation functions of various nuclides in the reactions $^{44}Ca+^{248}Cm$. The calculation of the maxima of the excitation functions is described in the text.

Nuclide	E_{max}(exp) (MeV)	E_{max}(calc) (MeV)	Nuclide	E_{max}(exp) (MeV)	E_{max}(calc) (MeV)
	$Z_{prod} \leq Z_{target}$			$Z_{prod} > Z_{target}$	
Th 227	234	<234	Bk 244	298	246
			245	298	<234
U 230	254	<234	246	298	257
237	>320	231	248*m*	298	>320
			250	>320	>320
Pu 243	>320	273			
245	>320	>320	Cf 246	276	<234
246	>320	>320	247	276	234
			248	276	<234
Am 240	254	239	250	254	253
244*g*	287	283	252	276	309
245	>320	320	253	276	>320
246*g*,*m*	>320	>320			
247	>320	>320	Es 250*g*,*m*	254,276	304
			251	276	302
Cm 249	>320	>320	252	276	>320
			253	298	296
			254*m*	298	>320
			Fm 252	254	249
			253	276	281
			254	254	256
			256	254	266

The excitation functions measured for above-target products in the reactions of $^{40,48}Ca+^{248}Cm$ were discussed in Ref. [6]. The excitation functions measured in the reactions of $^{40}Ca+^{248}Cm$ for isotopes of Bk, Cf, Es, and Fm were all very similar. The highest cross sections were observed for the near barrier energy, then decreased slowly, but not more than a factor of 2 with increasing projectile energy to 60 MeV above the barrier. The excitation functions for the production of isotopes of Bk, Cf, Es, and Fm for ^{48}Ca bombardments exhibited a maximum at an energy about 20 MeV above the Coulomb barrier and then decreased slowly up to energies 80 MeV above the Coulomb barrier. The observed threshold energies were consistent with the calculated positive reaction energies for ^{40}Ca bombardments and the negative reaction energies for ^{48}Ca bombardments (Table VI). Since the fission barriers for the measured actinide nuclides are only 5–6 MeV [56,57], the extra projectile energy was not manifested as excitation energy of the target-like products.

The excitation functions measured for target-like products in the reactions of $^{44}Ca+^{248}Cm$ are plotted in Figs. 3–8. The lines connecting the data points for a given isotope are intended only to guide the eye; dashed lines indicate excitation functions where actual cross sections have not been measured at all bombarding energies. The excitation functions for isotopes of Cm, Am, Pu, U, and Th all are similar in shape and show a more or less pronounced increase over the investigated energy range, except for the neutron-deficient nuclides ^{230}U and ^{227}Th. The sharp decrease of the cross sections for these two nuclides, that occurs at incident energies only 0–20 MeV above the barrier, seems to indicate dramatic losses of reaction products due to deexcitation by fission processes. The calculated excitation energies are about 20 MeV higher for these nuclides than in the $^{48}Ca+^{248}Cm$ system.

TABLE VIII. Energy of experimental and calculated maxima for the excitation functions of below-target nuclides in the reactions $^{40}Ca+^{248}Cm$. The calculation of the maxima of the excitation functions is described in the text.

Nuclide	E_{max}(exp) (MeV)	E_{max}(calc) (MeV)	Nuclide	E_{max}(exp) (MeV)	E_{max}(calc) (MeV)
Am 240	254	<233	Pu 236	<254	<233
244*g*	>289	<233			
245	>289	284	U 230	254	<233
246*g*	>289	>289			
			Th 227	<233	<233

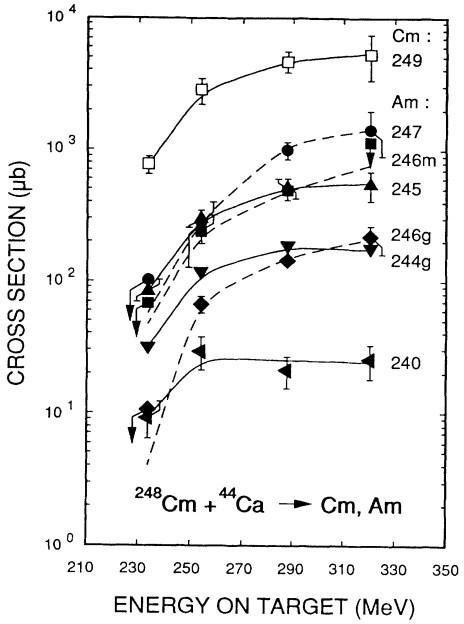

FIG. 3. Excitation functions for Cm and Am isotopes produced in bombardments of ^{248}Cm with ^{44}Ca projectiles. Data points are connected by lines to guide the eye.

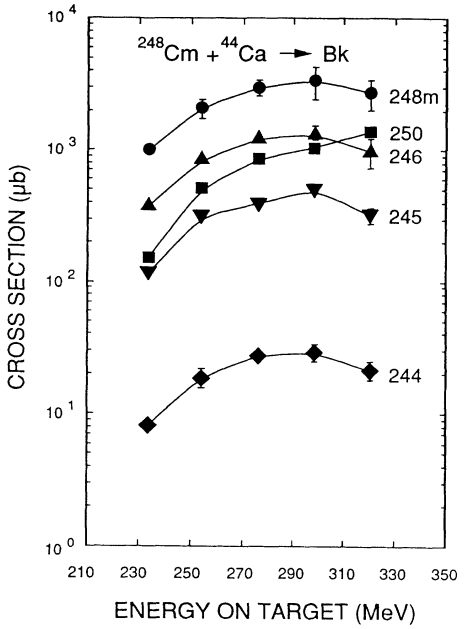

FIG. 5. Excitation functions for Bk isotopes produced in bombardments of ^{248}Cm with ^{44}Ca projectiles.

Another possible explanation could be the fact that the kinematic limitations of our target and catcher foil arrangement may contribute to losses of target-like reaction products. However, similar losses would be expected in all of the three investigated systems. The excitation functions measured for above-target products all show similar shapes. For most of the isotopes the maxima occur at about 70 MeV above the Coulomb barrier for Bk isotopes, at about 40 MeV for Cf and Es isotopes, and at about 20 MeV for Fm isotopes.

The excitation functions for below-target nuclides in the reactions of ^{40}Ca+^{248}Cm are shown in Fig. 9; the observed and calculated maxima of the excitation functions are given in Table VIII. The shapes of the excitation functions for below-target nuclides in the reactions of ^{40}Ca+^{248}Cm are similar to those measured in the

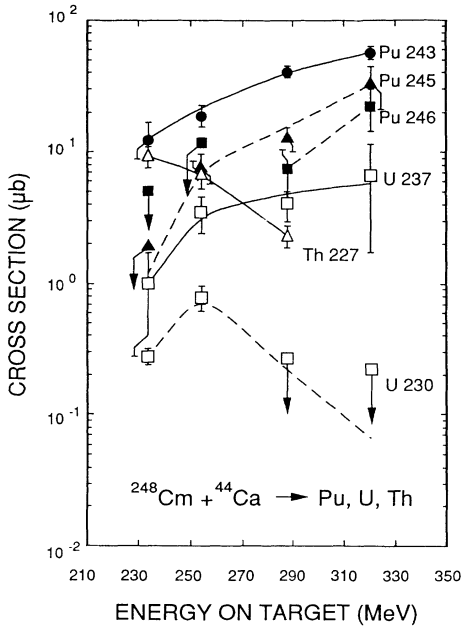

FIG. 4. Excitation functions for Pu, U, and Th isotopes produced in bombardments of ^{248}Cm with ^{44}Ca projectiles.

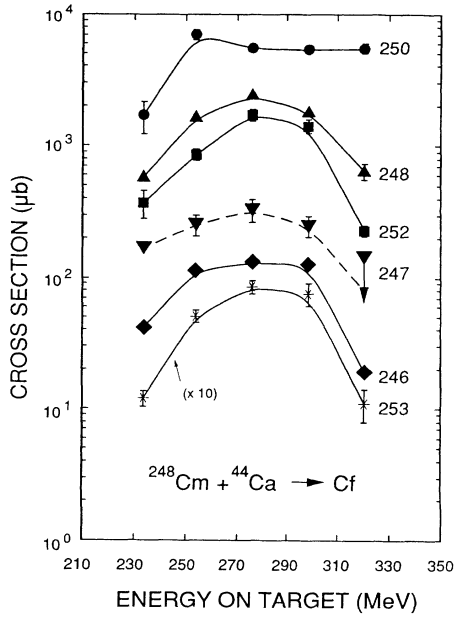

FIG. 6. Excitation functions for Cf isotopes produced in bombardments of ^{248}Cm with ^{44}Ca projectiles. The yields of ^{253}Cf have been multiplied by a factor of 10.

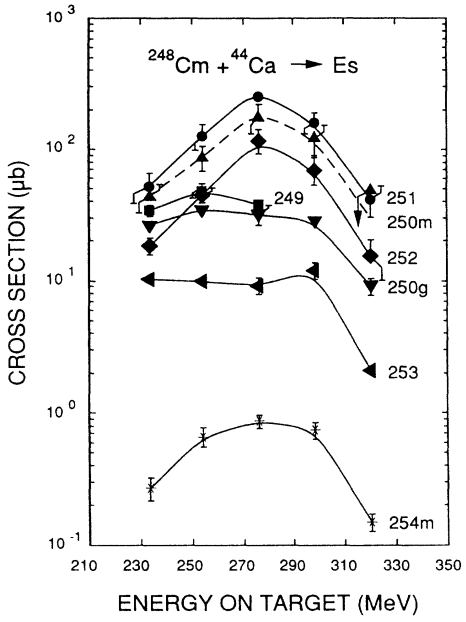

FIG. 7. Excitation functions for Es isotopes produced in bombardments of ^{248}Cm with ^{44}Ca projectiles. Dashed lines denote excitation functions where actual cross sections have not been measured at all bombarding energies.

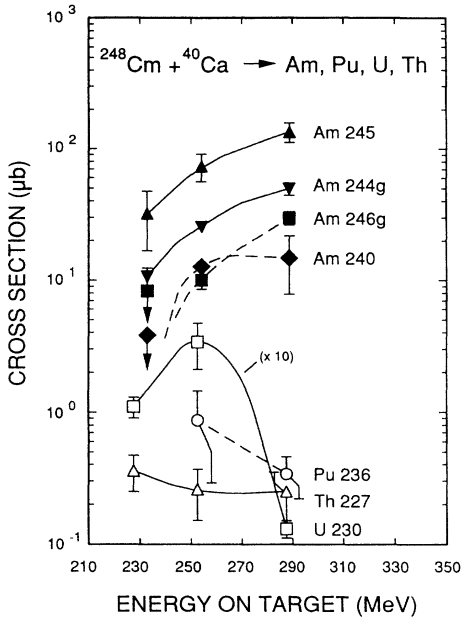

FIG. 9. Excitation functions for Am, Pu, U, and Th isotopes produced in bombardment of ^{248}Cm with ^{40}Ca projectiles. Data of ^{236}Pu, ^{230}U, and ^{227}Th from Ref. [30]. The yields of ^{230}U have been multiplied by a factor of 10.

^{44}Ca+^{248}Cm system. Again, the decreasing cross sections for neutron-deficient nuclides ^{236}Pu, ^{230}U, and ^{227}Th seem to indicate losses of reaction products due to prompt fission at higher incident energies.

In general, the maxima of the neutron-deficient isotopes were predicted by the simple model [43] with poor accuracy, whereas for the neutron-rich isotopes better agreement with the experimental results was obtained. The neutron-deficient isotopes may not reflect the initially formed reaction products, but rather secondary products after neutron evaporation or fission processes. The dissipation of kinetic energy among the products may contribute more or less to the total excitation energy than proposed previously in this section. A dissipation mechanism that relies more strongly on the number of protons transferred, rather than the number of exchanged nucleons, might yield more accurate predictions of the maxima of the excitation functions.

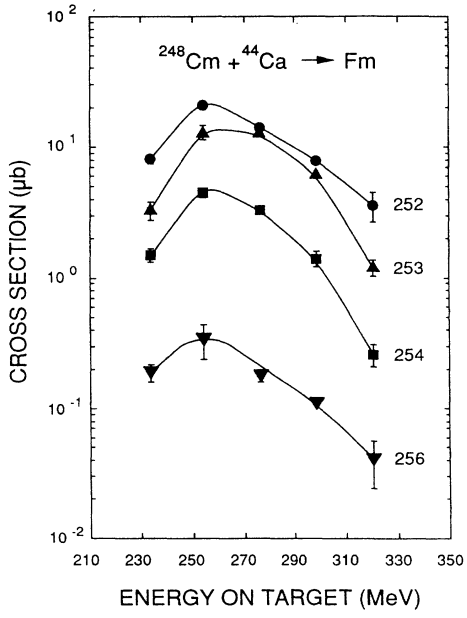

FIG. 8. Excitation functions for Fm isotopes produced in bombardments of ^{248}Cm with ^{44}Ca projectiles.

E. Element yields

Under the assumption that the few experimentally determined FWHM's for the Guassian below-target isotopic distributions in the experiments with ^{48}Ca are generally applicable [9], and with the estimated most probable mass numbers $\langle A \rangle_Z$ estimated from the PES calculations and the measured $\langle A' \rangle_Z$, the isotopic distributions can be constructed, even if only one isotope of an element has been measured. In Fig. 10 the elemental yields $(d\sigma/dZ)$ in experiments with ^{40,44,48}Ca+^{248}Cm are shown. The energy in all experiments corresponded to about $1.1E_{\text{Coul}}$. The most striking differences concern the yields of below-target elements. In the experiments with ^{48}Ca rather constant and high elemental yields of about 1 mb are observed. In experiments with ^{44}Ca the elemental yields are lower by more than one order of magnitude and are less than 100 μb for U and Th. The elemental yields for below-target elements in the reactions with ^{40}Ca are another order of magnitude lower and reach a few μb for U and Th.

Two reasons may account for this unexpected behavior: (a) The calculated maximum excitation energies in

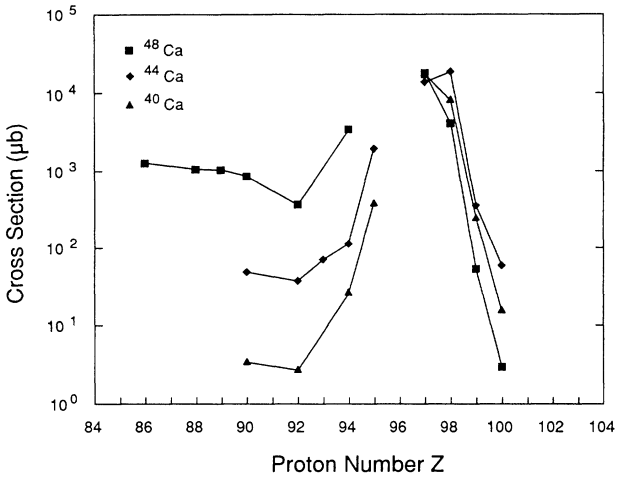

FIG. 10. Integrated element yields in the reactions of ^{40,44,48}Ca projectiles with ^{248}Cm at a bombarding energy corresponding to $1.1E_{\mathrm{Coul}}$. ^{48}Ca data from Refs. [6,9] and ^{40}Ca data partly from Refs. [6,30].

transfer reactions for below-target products are about 10 MeV higher in the reactions with ^{44}Ca and about 20 MeV higher in the reactions with ^{40}Ca compared to ^{48}Ca. The residual excitation of the heavy fragments is probably higher in the reactions with ^{44}Ca and especially ^{40}Ca due to the differences in the Q_{gg} values. Therefore, the observed differences in the below-target yields of the three reaction systems may be due to losses by prompt fission and neutron emission. The excitation functions measured for U and Th isotopes for the reactions with ^{40,44}Ca support this hypothesis. Unfortunately, no excitation functions for below-target elements are available for ^{48}Ca induced reactions. (b) The below Pa elements are probably formed in very asymmetric quasifission reactions. The shape of the Z (or A) distribution of the capture cross section between the quasielastic transfer peaks strongly affects the yields observed for very asymmetric quasifission reactions. Töke *et al.* [27] and Shen *et al.* [29] have shown that, depending on the fusion hindrance of the investigated system and the extrapush energies needed to induce capture reactions, different fragment distributions are found. The absence of fusion hindrance allows the formation of a fully equilibrated compound nucleus which deexcites by fission and/or neutron emission. A narrow mass distribution is observed for symmetric divisions. Very asymmetric quasifission does not occur. In a system with considerable fusion hindrance, such as ^{48}Ca+^{238}U, which is very similar to the ^{48}Ca+^{248}Cm system, Töke *et al.* [27] have found that the distribution of fragment masses was essentially flat between the quasielastic transfer peaks. A broad mass distribution has been observed in the reactions of ^{40}Ca+^{238}U (Ref. [25]), but in contrast to the ^{48}Ca+^{238}U system the region of quasifission reactions was clearly separated by a prominent minimum from the quasielastic transfer products, suggesting a less strong dynamic suppression of compound nucleus formation. A similar transition may occur in the ^{40,44,48}Ca+^{248}Cm system where the low yields of below-target products in the reactions of ^{40,44}Ca reflect a different dynamic evolution of the interaction process. Apparently, the fusion of ^{40}Ca+^{248}Cm is less hindered than the fusion of ^{48}Ca+^{248}Cm, with ^{44}Ca+^{248}Cm being intermediate. The suppression of compound nucleus formation has been interpreted to be one of the reasons why no superheavy elements were observed in the ^{48}Ca+^{248}Cm reaction [9,22].

For above-target elements the lowest yields occur for the reactions with ^{48}Ca (Fig. 10). The use of ^{40}Ca projectiles leads to elemental yields that are larger than with ^{48}Ca by a factor of about 5 for Es and Fm. The yields for Bk and Cf are not significantly different. Similarly, the yields drop with each additional proton transferred to the target nucleus. For the reactions with ^{44}Ca, the Cf yields are even higher than the Bk yields. In all the reactions with ^{248}Cm targets studied so far [3–7,10,15–17] similarly high Cf yields have only been observed in the reactions of ^{40}Ar+^{248}Cm (Ref. [15]). The transfer of 2 and also 4 protons seems to be favored in these systems. The enhancement in yield for even transfers of protons has been extensively studied by von Oertzen *et al.* [59] and was shown to occur in many different projectile-target combinations. It is further interesting to compare the measured $1p$ and $2p$ transfer cross sections, with a system where less fissile products are formed. Gardès *et al.* [55] have measured quasielastic excitation functions for a number of projectiles with ^{209}Bi targets. They found that almost independent of the projectile the $1p$ transfer cross sections amounted to 50 to 80 mb, whereas the $2p$ transfer cross sections were on the order of 10 mb for projectiles with $Z > 20$. This result implies that in the case of the $1p$ transfer to ^{248}Cm only about 10% of the formed Bk isotopes survive fission, whereas the $2p$ transfer occurs essentially cold, especially in the reactions with ^{44}Ca and ^{40}Ar projectiles.

Generally, in the reactions of ^{40}Ca and ^{44}Ca a trend towards asymmetric mass divisions, at least for the initial transfers, is obvious, whereas in the reactions with ^{48}Ca no preferential transfer direction exists. A similar effect was observed in the reactions of 340-MeV ^{40}Ca+^{238}U and 425-MeV ^{48}Ca+^{238}U (Refs. [18,20]), where the evolution of the width of the Z distributions was studied for various energy losses. In the case of ^{48}Ca no preferential transfer of protons was observed up to energy losses of about 75 MeV. For more inelastic interactions a weak trend towards symmetric mass division was observed. In the reactions of ^{40}Ca a preferential transfer of protons from the projectile to the target nucleus persisted up to energy losses of about 60 MeV. Then gradually proton transfers in the opposite direction took place in more inelastic interactions. A possible explanation for this behavior was discussed by Planeta *et al.* [21]. It may be that there exists a significant neutron skin for actinide nuclei, and the neck region that develops during the early stages of the interaction will be highly neutron rich. The surface density of neutrons in the projectile is much smaller than for the target nucleus, especially in neutron-deficient projectiles such as ^{40}Ca. There will be a strong driving force for protons to flow from the projectile into this neutron-rich neck region in order to mini-

mize the total isospin. This behavior leads to a preferential transfer of protons from the projectile to the neutron-rich target nucleus in the early stages of the interaction.

A series of open questions exist which cannot be answered unambiguously on the basis of the present data. Further experiments are needed to determine whether dynamic effects play an important role. This could be done by a complete investigation of the projectile-like and quasifission products with radiochemical methods, similar to that of Kratz *et al.* [1], who investigated the $^{40}Ar+^{238}U$ system. However, the main disadvantage of radiochemical methods lies in the loss of information about the kinetic energy of the reaction products, which is one of the most important parameters in describing the evolution of a heavy ion reaction [18–21]. An investigation of projectile-like reaction products with a *E-dE* counter telescope technique with high Z, A, and kinetic-energy resolution would yield important additional information [18,20,21]. It would also be interesting to measure cross sections for Md and No isotopes in order to see whether the yield enhancement for cold transfers of proton pairs persists.

V. SUMMARY

The reactions of ^{40}Ca and ^{44}Ca with ^{248}Cm were investigated at energies near the Coulomb barrier by measuring cross sections for target-like reaction products using radiochemical methods. Our results augment the data available on the interactions of ^{40}Ca and ^{48}Ca with ^{248}Cm (Refs. [6,9,30]), and allow an intercomparison of the three systems. The following conclusions can be drawn based on the discussion presented in Sec. IV.

(1) Similar FWHM's for the Gaussian isotopic distributions were observed for the interactions of $^{40,44,48}Ca$ projectiles with ^{248}Cm. The narrow (FWHM$\approx$2.5 mass numbers) isotopic distributions of above-target elements have been assigned to quasielastic reactions. Similar widths have been observed independently of the mass and charge of the projectiles. In contrast, the below-target isotopic distributions for all three systems are much broader (FWHM$\approx$5–6 mass numbers); they have been attributed to deeply inelastic and/or asymmetric quasifission reactions.

(2) The maxima of the isotopic distributions $\langle A' \rangle_Z$ in the reactions of $^{48}Ca+^{248}Cm$ were shown [9] to closely follow the minimum of the PES, indicating that the observed nuclides above and below the target nucleus must have been formed essentially cold, since neutron evaporation processes would have shifted the location of the $\langle A' \rangle_Z$ to the neutron-deficient side of the PES valley. In reactions of $^{40,44}Ca$ ions with ^{248}Cm a transfer of 4 to 5 protons in either direction was required to reach the minimum in PE. Due to the fact that all observed $\langle A' \rangle_Z$ are located on the neutron-rich side of the PES, the measured nuclides must have been formed cold. The equilibration of the N/Z ratio gradually occurs by the transfer of protons and not of neutrons, or a strong drift of the $\langle A' \rangle_Z$ towards the minimum of the PES would have resulted.

(3) The different neutron numbers of the projectiles are only partly reflected in the target-like reaction products. The differences between the positions of the $\langle A' \rangle_Z$ for Bk, Cf, and Es are smaller than 1 mass number between the reactions of ^{40}Ca and ^{44}Ca, and about 1 to 2 mass numbers between those of ^{40}Ca and ^{48}Ca. The $\langle A' \rangle_Z$ of the Fm distributions differs by less than 1 mass number between ^{40}Ca and ^{44}Ca reactions and by about 3 mass numbers between those of ^{40}Ca and ^{48}Ca. Similarly the $\langle A' \rangle_Z$ of below-target isotopic distributions differs by not more than 2 to 4 mass numbers.

(4) The model of Ref. [43] yields information about the energy available for fragment excitation. The model was shown to predict essentially correct excitation energies for below- as well as above-target elements if it was assumed that the heavy fragment carried the total calculated excitation energy. The inclusion of fragment deformations results in excitation energies that are about 70 MeV higher; however, there are indications [9] that for asymmetric quasifission reactions the excitation energy is divided between the heavy and the light fragment in the ratio $E_h^*/E_l^* \approx 0.2-0.3$. The differences in excitation energy in the three systems $^{40,44,48}Ca+^{248}Cm$ are mainly due to the differences in the Q_{gg} values.

(5) Using the model of Ref. [43] the maxima of the excitation functions were predicted with poor accuracy for neutron-deficient isotopes, whereas for neutron-rich isotopes better agreement with the experimental results was obtained. In general, the excess kinetic energy did not contribute strongly to the excitation energy of the heavy reaction products. A dissipation mechanism that relies more strongly on the number of protons transferred, rather than the total number of nucleons, might yield more accurate predictions.

(6) Considerable differences exist in the elemental yields ($d\sigma/dZ$) of the reactions of $^{40,44,48}Ca+^{248}Cm$ for below-target as well as for above-target elements. Differences of about two orders of magnitude were observed in the yields of below-target elements between the reactions of ^{40}Ca and ^{48}Ca, whereas the differences for above-target yields were largest between the reactions of ^{44}Ca and ^{48}Ca. The following may account for the smaller below-target elemental yields in the reactions of ^{44}Ca, and especially ^{40}Ca, with ^{248}Cm than in the reactions of ^{48}Ca. (a) Prompt fission and/or neutron emission of excited primary reaction products may contribute to substantial losses of below-target reaction products in the reactions with $^{40,44}Ca$. (b) The element yields of asymmetric quasifission reactions are strongly influenced by the FWHM of the charge (or mass) distribution of the quasifission process. An enhanced compound-nucleus fission type reaction may yield a pronounced minimum between the quasifission charge (or mass) distribution and the quasielastic transfer peaks, whereas a dynamic suppression of the compound-nucleus formation yields enhances the yield of deeply inelastic interactions. (c) Kinematic limitations of our target and catcher foil arrangement have been discussed. On the basis of these calculations, losses of below-target reaction products cannot be

ruled out, but should be similar in all three systems.

The differences in above-target yields can be explained by different reaction energies in the three systems $^{40,44,48}Ca+^{248}Cm$. Negative reaction energies seem to hinder the formation of above-target nuclides in the reactions of $^{48}Ca+^{248}Cm$, whereas the slightly positive reaction energies in the interactions of $^{44}Ca+^{248}Cm$ favor the formation of above-target nuclides without introducing too much excitation energy. In the reactions with ^{44}Ca a very pronounced enhancement of 2 and 4 proton transfers was observed.

(7) The preferential transfer of protons from the projectile to the target in the reactions of $^{40,44}Ca+^{248}Cm$ may be explained by the isospin driving force, where the neutron-rich neck region that develops during the interactions favors the transfer of protons from the projectile to the target nucleus.

ACKNOWLEDGMENTS

We would like to thank the crew of the 88-Inch Cyclotron for their assistance and for providing high intensity beams of ^{40}Ca and ^{44}Ca. We are indebted for the use of the ^{248}Cm to the Division of Chemical Sciences, Office of Basic Energy Sciences, U.S. Department of Energy, through the transplutonium element production facilities at the Oak Ridge National Laboratory. Discussions with H.W. Gäggeler, J.V. Kratz, and U.W. Scherer are gratefully acknowledged. We wish to thank M. Lerch for furnishing unpublished $^{40}Ca+^{248}Cm$ results. This work was supported in part by the Office of Energy Research, Division of Nuclear Physics of the Office of High Energy and Nuclear Physics of the U.S. Department of Energy under Contract No. DE-AC03-76SF00098 and the Swiss National Science Foundation.

[1] J. V. Kratz, J. O. Liljenzin, A. E. Norris, and G. T. Seaborg, Phys. Rev. C **13**, 2347 (1976).

[2] M. Schädel, J. V. Kratz, H. Ahrens, W. Brüchle, G. Franz, H. Gäggeler, I. Warnecke, G. Wirth, G. Herrmann, N. Trautmann, and M. Weis, Phys. Rev. Lett. **41**, 469 (1978).

[3] M. Schädel, W. Brüchle, H. Gäggeler, J. V. Kratz, K. Sümmerer, G. Wirth, G. Herrmann, R. Stakemann, G. Tittel, N. Trautmann, J. M. Nitschke, E. K. Hulet, R. W. Lougheed, R. L. Hahn, and R. L. Ferguson, Phys. Rev. Lett. **48**, 852 (1982).

[4] D. Lee, H. R. von Gunten, B. Jacak, M. J. Nurmia, Yuan-Fang Liu, Cheng Luo, G. T. Seaborg, and D. C. Hoffman, Phys. Rev. C **25**, 286 (1982).

[5] D. Lee, K. J. Moody, M. J. Nurmia, G. T. Seaborg, H. R. von Gunten, and D. C. Hoffman, Phys. Rev. C **27**, 2656 (1983).

[6] D. C. Hoffman, M. M. Fowler, W. R. Daniels, H. R. von Gunten, D. Lee, K. J. Moody, K. Gregorich, R. Welch, G. T. Seaborg, W. Brüchle, M. Brügger, H. Gäggeler, M. Schädel, K. Sümmerer, G. Wirth, T. Blaich, G. Herrmann, N. Hildebrand, J. V. Kratz, M. Lerch, and N. Trautmann, Phys. Rev. C **31**, 1763 (1985).

[7] K. J. Moody, D. Lee, R. B. Welch, K. E. Gregorich, G. T. Seaborg, R. W. Lougheed, and E. K. Hulet, Phys. Rev. C **33**, 1315 (1986).

[8] M. Schädel, W. Brüchle, H. Gäggeler, K. J. Moody, D. Schardt, K. Sümmerer, E. K. Hulet, A. D. Dougan, R. J. Dougan, J. H. Landrum, R. W. Lougheed, J. F. Wild, and G. D. O'Kelly, Phys. Rev. C **33**, 1547 (1986).

[9] H. Gäggeler, W. Brüchle, M. Brügger, M. Schädel, K. Sümmerer, G. Wirth, J. V. Kratz, M. Lerch, T. Blaich, G. Herrmann, N. Hildebrand, N. Trautmann, D. Lee, K. J. Moody, K. E. Gregorich, R. B. Welch, G. T. Seaborg, D. C. Hoffman, W. R. Daniels, M. M. Fowler, and H. R. von Gunten, Phys. Rev. C **33**, 1983 (1986).

[10] R. B. Welch, K. J. Moody, K. E. Gregorich, D. Lee, and G. T. Seaborg, Phys. Rev. C **35**, 204 (1987).

[11] K. E. Gregorich, K. J. Moody, D. Lee, W. K. Kot, R. B. Welch, P. A. Wilmarth, and G. T. Seaborg, Phys. Rev. C **35**, 2117 (1987).

[12] R. M. Chasteler, R. A. Henderson, D. Lee, K. E. Gregorich, M. J. Nurima, R. B. Welch, and D. C. Hoffman, Phys. Rev. C **36**, 1820 (1987).

[13] K. J. Moody, W. Brüchle, M. Brügger, H. Gäggeler, B. Haefner, M. Schädel, K. Sümmerer, H. Tetzlaff, G. Herrmann, N. Kaffrell, J. V. Kratz, J. Rogowski, N. Trautmann, M. Skålberg, G. Skarnemark, J. Alstadt, and M. M. Fowler, Z. Phys. A **328**, 417 (1987).

[14] U. W. Scherer, W. Brüchle, M. Brügger, C. Frink, H. Gäggeler, G. Herrmann, J. V. Kratz, K. J. Moody, M. Schädel, K. Sümmerer, N. Trautmann, and G. Wirth, Z. Phys. A **335**, 421 (1990).

[15] J. D. Leyba, R. A. Henderson, H. L. Hall, C. M. Gannett, R. B. Chadwick, K. R. Czerwinski, S. A. Kreek, G. R. Haynes, K. E. Gregorich, D. M. Lee, M. J. Nurmia, and D. C. Hoffman, Phys. Rev. C **41**, 2092 (1990).

[16] J. D. Leyba, Ph.D. thesis, Lawrence Berkeley Laboratory Report LBL-**29540**, 1990.

[17] J. D. Leyba, R. A. Henderson, H. L. Hall, K. R. Czerwinski, B. A. Kakhodayan, S. A. Kreek, E. K. Brady, K. E. Gregorich, D. M. Lee, M. J. Nurmia, and D. C. Hoffman, Phys. Rev. C **44**, 1850 (1991).

[18] R. T. de Souza, J. R. Huizenga, and W. U. Schröder, Phys. Rev. C **37**, 1901 (1988).

[19] H. Freiesleben and J. V. Kratz, Phys. Rep. **106**, 1 (1984).

[20] R. T. de Souza, W. U. Schröder, J. R. Huizenga, J. Töke, S. S. Datta, and J. L. Wile, Phys. Rev. C **39**, 114 (1989).

[21] R. Planeta, S. H. Zhou, K. Kwiatkowski, W. G. Wilson, V. E. Viola, H. Breuer, D. Benton, F. Khazaie, R. J. McDonald, A. C. Mignerey, A. Weston-Dawkes, R. T. de Souza, J. R. Huizenga, and W. U. Schröder, Phys. Rev. C **38**, 195 (1988).

[22] P. Armbruster, Y. K. Agarwal, W. Brüchle, M. Brügger, J. P. Dufour, H. Gäggeler, F. P. Hessberger, S. Hofmann, P. Lemmertz, G. Münzenberg, K. Poppensieker, W. Reisdorf, M. Schädel, K.-H. Schmidt, J. H. R. Schneider, W. F. W. Schneider, K. Sümmerer, D. Vermeulen, G. Wirth, A. Ghiorso, K. E. Gregorich, D. Lee, M. Leino, K. J. Moody, G. T. Seaborg, R. B. Welch, P. Wilmarth, S. Yashita, C. Frink, N. Greulich, G. Herrmann, U. Hickmann, N. Hildebrand, J. V. Kratz, N. Trautmann, M. M. Fowler, D. C. Hoffman, W. R. Daniels, H. R. von Gunten, and H. Dornhöfer, Phys. Rev. Lett. **54**, 406 (1985).

[23] H. W. Gäggeler, Paul Scherrer Institut Report, PSI-14, 1988.
[24] H. Sann, R. Bock, Y. T. Chu, A. Gobbi, A. Olmi, U. Lynen, W. Müller, S. Bjornholm, and H. Esbensen, Phys. Rev. Lett. **47**, 1248 (1981).
[25] R. Bock, Y. T. Chu, M. Dakowski, A. Gobbi, E. Grosse, A. Olmi, H. Sann, D. Schwalm, U. Lynen, W. Müller, S. Bjornholm, H. Esbensen, W. Wölfli, and E. Morenzoni, Nucl. Phys. **A388**, 334 (1982).
[26] K. Lützenkirchen, J. V. Kratz, W. Brüchle, H. Gäggeler, K. Sümmerer, and G. Wirth, Z. Phys. A **317**, 55 (1984).
[27] J. Töke, R. Bock, G. X. Dai, A. Gobbi, S. Gralla, K. D. Hildenbrand, J. Kuzminski, W. F. J. Müller, A. Olmi, H. Stelzer, B. B. Back, and S. Bjornholm, Nucl. Phys. **A440**, 327 (1985).
[28] H. Keller, R. Bellwied, K. Lützenkirchen, J. V. Kratz, W. Brüchle, H. Gäggeler, K. J. Moody, M. Schädel, and G. Wirth, Z. Phys. A **328**, 255 (1987).
[29] W. Q. Shen, J. Albinski, A. Gobbi, S. Gralla, K. D. Hildenbrand, N. Herrmann, J. Kuzminski, W. F. J. Müller, H. Stelzer, J. Töke, B. B. Back, S. Bjornholm, and S. P. Sorensen, Phys. Rev. C **36**, 115 (1987).
[30] M. Lerch, private communication
[31] D. H. E. Gross and K. M. Hartmann, Phys. Rev. C **24**, 2526 (1981).
[32] *Table of Isotopes*, 7th ed., edited by E. Browne, J. M. Dairiki, R. E. Doebler, C. M. Lederer, and V. S. Shirley (Wiley, New York, 1978).
[33] F. Hubert, R. Bimbot, and H. Gauvin, At. Data Nucl. Data Tables **46**, 1 (1990).
[34] J. S. Blair, Phys. Rev. **95**, 1218 (1954).
[35] A. Türler, F. Wegmüller, H. R. von Gunten, K. E. Gregorich, D. Lee, D. C. Hoffman, and M. M. Fowler, Radiochim. Acta **43**, 149 (1988).
[36] M. M. Fowler, W. R. Daniels, H. R. von Gunten, H. Gäggeler, D. C. Hoffman, D. Lee, K. Gregorich, K. J. Moody, M. Lerch, G. Herrmann, and N. Trautmann, Radiochim. Acta **40**, 75 (1986).
[37] A. Türler, Ph.D. thesis, Universität Bern, 1989.
[38] R. F. Mitchell, Anal. Chem. **32**, 326 (1960).
[39] J. T. Routti and S. G. Prussin, Nucl. Instrum. Methods **72**, 125 (1969).
[40] R. B. Welch, F. Gyger, D. T. Jost, H. R. von Gunten, and U. Krähenbühl, Nucl. Instrum. Methods A **269**, 615 (1988).
[41] K. E. Gregorich, Ph.D. thesis, Lawrence Berkeley Laboratory Report LBL-**20192**, 1985.
[42] L. A. Currie, Anal. Chem. **40**, 586 (1968).
[43] D. C. Hoffman and M. M. Hoffman, Los Alamos National Laboratory Report LA-UR-**82-824**, 1982.
[44] D. C. Hoffman and M. M. Hoffman, Lawrence Berkeley Laboratory Report LBL-**29502**, 1990.
[45] K. Lützenkirchen, J. V. Kratz, W. Brüchle, H. Gäggeler, K. Sümmerer, and G. Wirth, Z. Phys. A **317**, 55 (1984).
[46] J. R. Birkelund, L. E. Tubbs, J. R. Huizenga, J. N. De, and D. Sperber, Phys. Rep. **56**, 107 (1979).
[47] J. P. Bondorf, M. I. Sobel, and D. Sperber, Phys. Rep. **15C**, 83 (1974).
[48] J. Blocki, J. Randrup, W. J. Swiatecki, and C. F. Tsang, Ann. Phys. (N.Y.) **105**, 427 (1977).
[49] W. Wilcke, J. R. Birkelund, H. J. Wollersheim, A. D. Hoover, J. R. Huizenga, W. U. Schröder, and L. E. Tubbs, At. Data Nucl. Data Tables **25**, 389 (1980).
[50] W. D. Meyers, *Droplet Model of Atomic Nuclei* (IFI/Plenum, New York, 1977).
[51] S. Cohen and W. J. Swiatecki, Ann. Phys. (N.Y.) **19**, 67 (1962).
[52] V. E. Viola, K. Kwiatkowski, and M. Walker, Phys. Rev. C **31**, 1550 (1985).
[53] R. Vandenbosch, A. Lazzarini, D. Leach, D.-K. Lock, A. Ray, and A. Seamster, Phys. Rev. Lett. **52**, 1964 (1984).
[54] R. Planeta, K. Kwiatkowski, S. H. Zhouk, V. E. Viola, J. Breuer, M. A. McMahan, J. Randrup, and A. C. Mignerey, Phys. Rev. C **39**, 1197 (1989).
[55] D. Gardès, R. Bimbot, J. Maison, K. de Reilhac, M. F. Rivet, A. Fleury, F. Hubert, and Y. Llabador, Phys. Rev. C **18**, 1298 (1978).
[56] H. C. Britt, E. Cheifetz, D. C. Hoffman, J. B. Wilhelmy, R. J. Dupzyk, and R. W. Lougheed, Phys. Rev. C **21**, 761 (1980).
[57] G. T. Seaborg and W. D. Loveland, in *Treatise on Heavy Ion Science*, edited by D. A. Bromely (Plenum, New York, 1984).
[58] W. M. Howard and P. Möller, At. Data Nucl. Data Tables **25**, 219 (1980).
[59] W. von Oertzen, Phys. Rev. C **43**, 1522 (1991).